REFERENCES

[1] N. Marcuvitz, *Waveguide Handbook*. New York: McGraw Hill, 1951, ch. 5.

[2] R. E. Collin, *Field Theory of Guided Waves*. New York: Mc Graw Hill, 1960, ch. 8.

[3] K. Chang and P. J Khan, "Coupling between narrow transverse inductive strips in waveguides," *IEEE Trans. Microwave Theory Tech.*, vol. MTT-24, pp. 101–105, Feb. 1976.

[4] K. Chang and P. J. Khan, "Analysis of three narrow transverse strips in waveguide," in *1978 MTT-S Int Microwave Symp. Tech Dig.*, pp. 419–421.

[5] L. Lewin, "Solution of a singular integral equation over a multiple interval and applications to multiple strips, grids or waveguide diaphragms," *Electron Lett.*, vol. 2, pp 458–459, Dec. 1966.

[6] L. Lewin, *Theory of Waveguides*. New York: Wiley, 1974, chs. 6 and 7.

[7] L. Lewin, "The use of singular integral equation in the solution of waveguide problems," in *Advances in Microwaves*, vol. 1, L. Young, Ed New York: Academic Press, 1966, pp. 241–247.

[8] J. M. Jarem, "A multifilament method-of-moments solution for the input impedance of a probe-excited semi-infinite waveguide," *IEEE Trans Microwave Theory Tech.*, vol. MTT-35, pp. 14, Jan. 1987.

[9] Y. Leviatan, P G. Li, A T. Adams, and J. Perini, "Single-post inductive obstacles in rectangular waveguide," *IEEE Trans. Microwave Theory Tech.*, vol. MTT-31, pp. 806–811, Oct. 1983.

[10] Y Leviatan and G. S. Sheaffer, "Analysis of inductive dielectric posts in rectangular waveguide," *IEEE Trans. Microwave Theory Tech*, vol. MTT-35, pp. 48–59, Jan 1987.

[11] H Auda and R. F. Harrington, "Inductive posts and diaphragms of arbitrary shape and number in a rectangular waveguide," *IEEE Trans. Microwave Theory Tech.*, vol. MTT-32, pp. 606–613, June 1984.

[12] R. L Eisenhart and P. J. Khan, "Theoretical and experimental analysis of a waveguide mounting structure," *IEEE Trans Microwave Theory Tech.*, vol MTT-19, pp. 706–719, Aug 1971.

On Microwave Imagery Using Bojarski's Identity

TAH-HSIUNG CHU, MEMBER, IEEE, AND DING-BING LIN

Abstract — **In this paper, theoretical and experimental studies of microwave imagery of a perfectly conducting convex object of a size larger than the incident wavelength are presented. Experimental data were measured in the frequency range 4–10 GHz. Calculations were done with Bojarski's identity, one-dimensional Fourier inversion of the range-normalized scattered far field, and a back-projection algorithm. The images show the distribution of specular reflection regions on the surface of the object.**

I. INTRODUCTION

Bojarski's identity [1], [2] forms the basis for imaging a perfectly conducting convex object under physical optics approximations. The identity states that the characteristic function $\gamma(\boldsymbol{r})$ of the object, which is unity inside the scattering object and zero outside, and $\Gamma(\boldsymbol{p}) = 2\sqrt{\pi}\, p^{-2}[\rho(\boldsymbol{p}) + \rho^*(-\boldsymbol{p})]$ make up a Fourier transform pair where $\boldsymbol{r}$ is a position vector and $\boldsymbol{p} = -2k\hat{i}_k = p\hat{i}_p$, with $\hat{i}_k$ as the direction of the incident plane wave. The quantity $\rho(\boldsymbol{p})/p$ is the range-normalized scattered far field measured at all frequencies and viewing angles. However, in the case of microwave imaging, the reconstructed image becomes the derivative (or the edge information) of the characteristic function, since a band-pass version of $\Gamma(\boldsymbol{p})$ is measured [3], [4]. The image resolution is inversely proportional to the $\boldsymbol{p}$-space aperture (or area of $\Gamma(\boldsymbol{p})$) formed by varying frequency and viewing angle.

Manuscript received August 19, 1987; revised December 19, 1988. This work was supported by the National Science Council of the Republic of China under Grant NSC 77-0404-E002-40

The authors are with the Electrical Engineering Department, National Taiwan University, Taiwan, Republic of China.

IEEE Log Number 8927796.

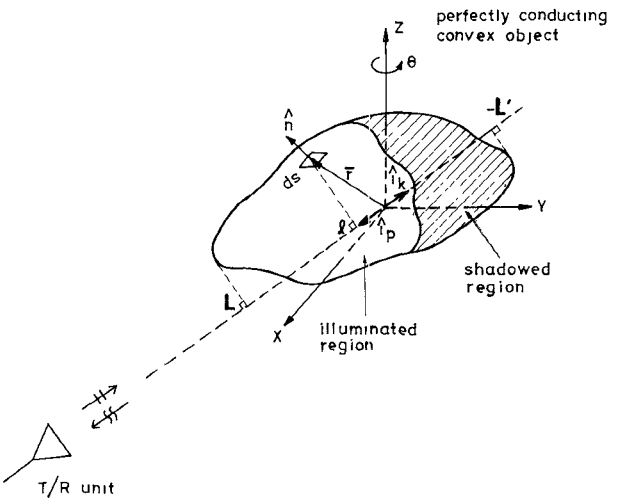

Fig. 1. The scattering geometry

It is known that the far field scattered by a metallic object subjected to coherent microwave illumination is determined by the relative positions of scattering centers on the illuminated portion of the object [5]. A scattering center is defined as the object structure that is observed in the backscattered field. For a smooth convex object of size larger than the incident wavelength, these scattering centers are the specular reflection regions distributed on the illuminated object surface.

The aim of this paper is to show analytically and experimentally that the reconstructed image of a convex metallic object using Bojarski's identity gives the distribution of these specular regions over the entire object surface.

II. THEORETICAL ANALYSIS

As a perfectly conducting convex object is illuminated with a monochromatic plane wave propagating in the direction $\hat{i}_k$, as shown in Fig. 1, its range-normalized backscattered far field under physical optics approximations can be expressed as [1], [2]

$$\frac{\rho(\boldsymbol{p})}{p} = \frac{j}{2\sqrt{\pi}} \int_{\hat{i}_p \cdot \hat{n} > 0} \left(\hat{i}_p \cdot \hat{n}\right) e^{-jp\,\hat{r}} \, dS(\boldsymbol{r}) \tag{1}$$

where $\boldsymbol{p} = -2k\hat{i}_k = p\hat{i}_p$, $k = 2\pi f/c$, $\hat{n}$ is the outward vector normal to the object surface $S(\boldsymbol{r})$, and the surface integral is over the illuminated portion of the object. In general, this surface integral cannot be integrated analytically. However, by adding $\rho(\boldsymbol{p})$ with $\rho^*(-\boldsymbol{p})$ measured with the transmitter/receiver (T/R) unit at the other side of the object and using the divergence theorem, one can obtain [1], [2]

$$\Gamma(\boldsymbol{p}) = \frac{2\sqrt{\pi}}{p^2}\left[\rho(\boldsymbol{p}) + \rho^*(-\boldsymbol{p})\right] = \int \gamma(\boldsymbol{r})\, e^{-jp\,\hat{r}}\, d\boldsymbol{r} \tag{2}$$

where $\gamma(\boldsymbol{r})$ is the characteristic function of the scattering object B, defined as

$$\gamma(\boldsymbol{r}) = \begin{cases} 1, & \boldsymbol{r} \text{ in B} \\ 0, & \boldsymbol{r} \text{ not in B.} \end{cases} \tag{3}$$

Equation (2) is known as Bojarski's identity [1], [2]. It shows that an image of the scattering object B can be reconstructed from the backscattered far field measured at all frequencies and viewing angles through the Fourier inversion. The reconstructed

image has a unity intensity inside the object according to (3), although the incident plane wave cannot penetrate a perfectly conducting object.

Note that in (1)

$$\left(\hat{i}_p \cdot \hat{n}\right) dS = dS_{\hat{i}_p} \tag{4}$$

is equal to the projection of the element of surface area dS onto the plane normal to the $\hat{i}_p$ axis, and

$$\boldsymbol{p} \cdot \boldsymbol{r} = p\hat{i}_p \cdot \mathbf{r} \equiv pl \tag{5}$$

where l is the projection length of the illuminated object element (or scattering center) at position $\boldsymbol{r}$ onto the $\hat{i}_p$ axis. Therefore, (1) becomes

$$\frac{\rho(p)}{p} = \frac{j}{2\sqrt{\pi}} \int e^{-jpl}\, dS_{\hat{i}_p} = \frac{j}{2\sqrt{\pi}} \int_0^L \frac{\partial S_{\hat{i}_p}}{\partial l} e^{-jpl}\, dl \tag{6}$$

where L is the maximum projection length of the illuminated portion of object on the $\hat{i}_p$ axis; $S_{\hat{i}_p} = 0$ for $l > L$, and $S_{\hat{i}_p} = S_{\hat{i}_p \max}$ for $l < 0$ (in the shadowed region).

Equation (6) shows that, under physical optics approximations, a line of $\rho(\boldsymbol{p})/p$ data recorded from one view is proportional to the one-dimensional Fourier transform of $\partial S_{\hat{i}_p}/\partial l$, i.e., the derivative (or discontinuities) of the object projection area $S_{\hat{i}_p}$ [5].

Since no discontinuities in $S_{\hat{i}_p}$ were assumed at the shadow boundary, and the object size is larger than the wavelength, the discontinuities of the cross-sectional area occur at specular regions (or scattering centers) on the illuminated surface of a smooth convex object. Therefore a set of one-dimensional projection images of the object scattering centers can be acquired from $\rho(\boldsymbol{p})/p$ data collected by varying the frequency and viewing angle. The range and angular resolutions are inversely proportional to, respectively, the bandwidth utilized and the span of viewing angle. The image of object scattering centers can be reconstructed from these one-dimensional projection images by using the back-projection algorithm developed in X-ray tomography [6].

However, one should note that the X-ray tomography is an incoherent system which records the one-dimensional projections of the X-ray absorptivity of the test object on the viewing aperture. The described imaging system, however, is a coherent system which records the backscattered far field of the object by varying the frequency at each viewing angle, and one-dimensional projection calculated from the Fourier inversion gives the profile of the object discontinuities along $\hat{i}_p$ axis according to (6).

The reconstructed image contains an ensemble of regions that represents the scattering center distribution on the illuminated portion of the object surface, and the intensity of each scattering center is proportional to the derivative of the projected area. Note, in the case of a flat surface, that the image intensity is proportional to the illuminated area. Similar results can be derived using the stationary phase method [7]; however, the stationary phase result is only valid for the curved surface. Using a comparison with the characteristic function $\gamma(\boldsymbol{r})$ defined in (3), which is unity inside the scattering object, we see that the reconstructed image using one-dimensional Fourier inversion and the back-projection algorithm of $\rho(\boldsymbol{p})/p$ data is different because it is represented by the distribution of scattering centers. However, when the scattering data are recorded in the microwave region, these two approaches will yield similar images, as discussed in the following.

From the slice-projection theorem [6], the one-dimensional Fourier inversion of a line of $\Gamma(\boldsymbol{p})$ data recorded from one view

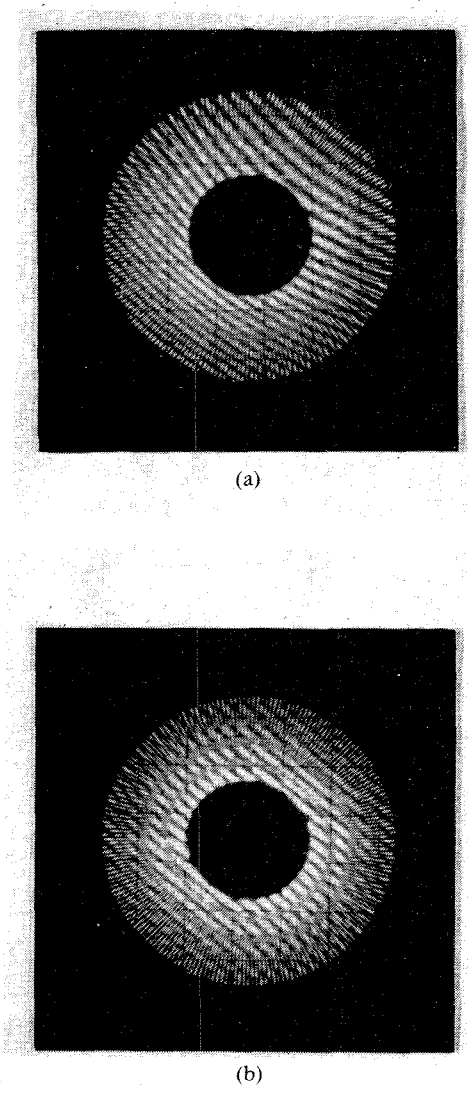

(a)

(b)

Fig. 2. Slices of the recorded $\boldsymbol{p}$-space data (real part) (a) $\rho(\boldsymbol{p})/p$ and (b) $\Gamma(\boldsymbol{p})$ of the metallic cylinder (the imaginary part data having a similar feature).

by varying the frequency (or p) gives the projection image of the cross-sectional area $S_{\hat{i}_p}$ of the object on the plane normal to the $\hat{i}_p$ axis; i.e.,

$$\Gamma(p) = \int_{-L'}^{L} S_{\hat{i}_p} e^{-jpl}\, dl \tag{7}$$

where $-L'$ is the maximum projection length of the shadow portion of the object on the $\hat{i}_p$ axis as shown in Fig. 1. In the case of microwave imagery, the measured data lie offset from the origin of the $\boldsymbol{p}$ space [8]. For example, in the experimental arrangement to be discussed in the next section, the frequency is swept from 4 GHz to 10 GHz; 1.68 rad/cm $\leqslant p \leqslant$ 4.19 rad/cm gives a band-pass version of $\Gamma(\boldsymbol{p})$. The reconstructed image from each line of $\Gamma(\boldsymbol{p})$ is then equivalent to the derivative of the projection cross-sectional area of the scattering object $\partial S_{\hat{i}_p}/\partial l$; however, it contains specular regions on the front and back surfaces. Therefore, as the scattering data are measured in the microwave range over $\theta = 360°$ around the object and the scattering convex object size is larger than the wavelength, the reconstructed images from $\rho(\boldsymbol{p})/p$ and $\Gamma(\boldsymbol{p})$ have the same features. In the case of a partial viewing angle, an image reconstructed from available $\rho(\boldsymbol{p})/p$ gives only the scattering centers on the

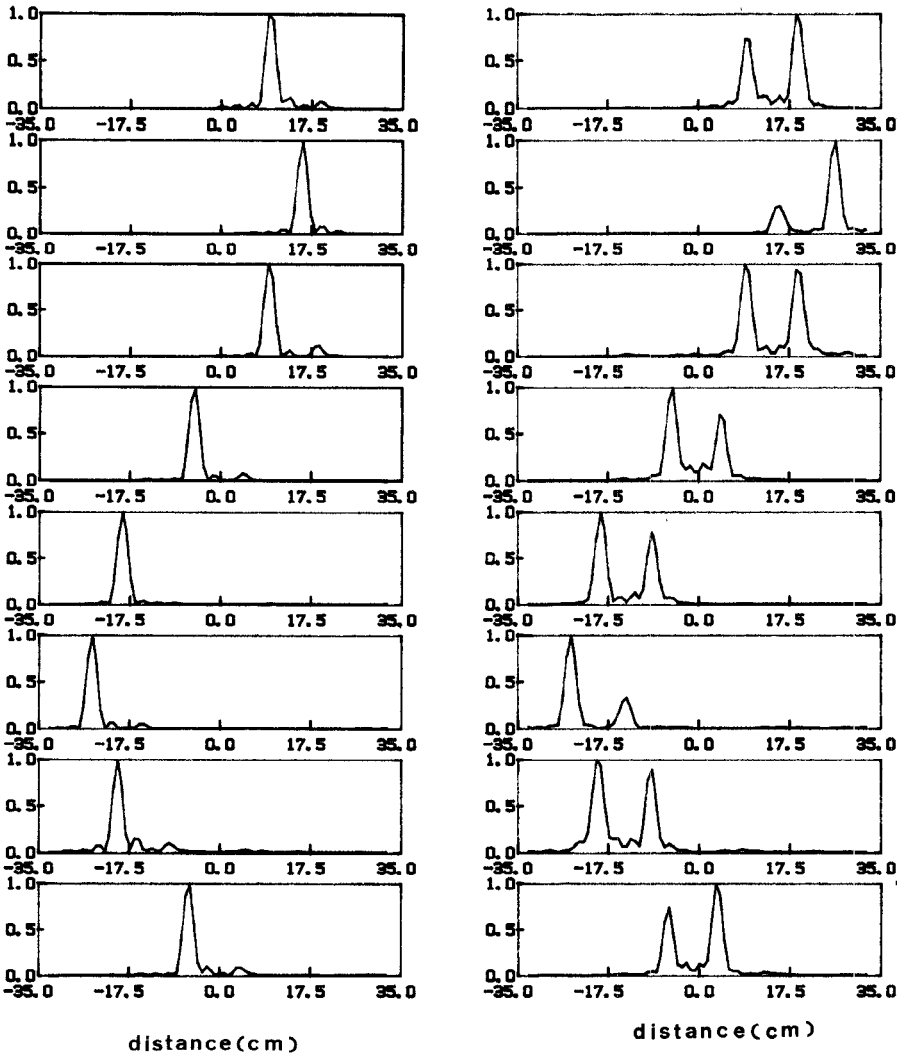

Fig 3. One-dimensional projection images obtained from (a) $\rho(p)/p$ and (b) $\Gamma(p)$ data at aspect angles $\theta = 0°$ to 315° with 45° intervals (from top to bottom). The vertical axis is the normalized intensity, and the horizontal axis is the distance in cm

illuminated surface. Experimental results obtained from the measured scattering data of a metallic cylinder will be discussed in the next section.

III. Experimental Results

In the measurement, a metallic cylinder with a length of 120 cm and a diameter of 11 cm is initially mounted in the direction of $\theta = 45°$ and 20 cm off the center of a computer-controlled positioner ($\theta = 0°$ being the direction of $\hat{i}_k$). The scattering effect from the cylinder's ends in negligible because the T/R unit points to the central region of the cylinder. The entire measurement sequence consists of angular positioning of the object in increments of 1.8° over 360°, incremental frequency tuning over 4–10 GHz, and digitization and storage of the amplitude and phase readings of the coherent receiver.

For each measurement, the sweep oscillator steps through the frequency range linearly in 80 steps and an HP8410B network analyzer records the cylinder backscattered field. The cylinder is then rotated to a new aspect angle and the frequency response measurement is repeated. Note the cylinder radius a (5.5 cm) is such that $4.62 \leqslant ka \leqslant 11.5$ for the frequency band employed in the measurement; i.e., the measurement is in the physical optics regime. The polarization of the T/R unit is along the cylinder axis direction.

Two slices of $\rho(p)/p$ and $\Gamma(p)$ data, shown in Fig. 2(a) and (b), are acquired. The p-space data are recorded in a polar format consisting of 200 radial lines, each corresponding to a frequency sweep and an angular range of 360° and each line containing 80 data points for a total of 16K complex values.

Shown in Fig. 3(a) and (b) are the results obtained by performing one-dimensional Fourier inversion of a line of $\rho(p)/p$ and $\Gamma(p)$ data at $\theta = 0°$ to 315° in 45° intervals. The sharp spikes shown in Fig. 3(a) represent the specular reflection region (or the scattering center) on the illuminated cylinder surface, which is $L = 20\cos(\theta - 45°) - 5.5$ cm, where 45° is the initial angle of the cylinder. The two-dimensional image shown in Fig. 4(a) is reconstructed from these one-dimensional projection images.

However, the two sharp spikes shown in Fig. 3(b) are obtained from one-dimensional Fourier inversion of $\Gamma(p)$ recorded from two observations at the opposite side of the cylinder according to (2). They represent the derivative of the projection cross-sectional area or the projection of the cylinder front and back edges (or specular regions). The distance between two spikes is equal to the cylinder diameter. The first spike is at the same location as shown in Fig. 3(a), and the second spike corresponds to the

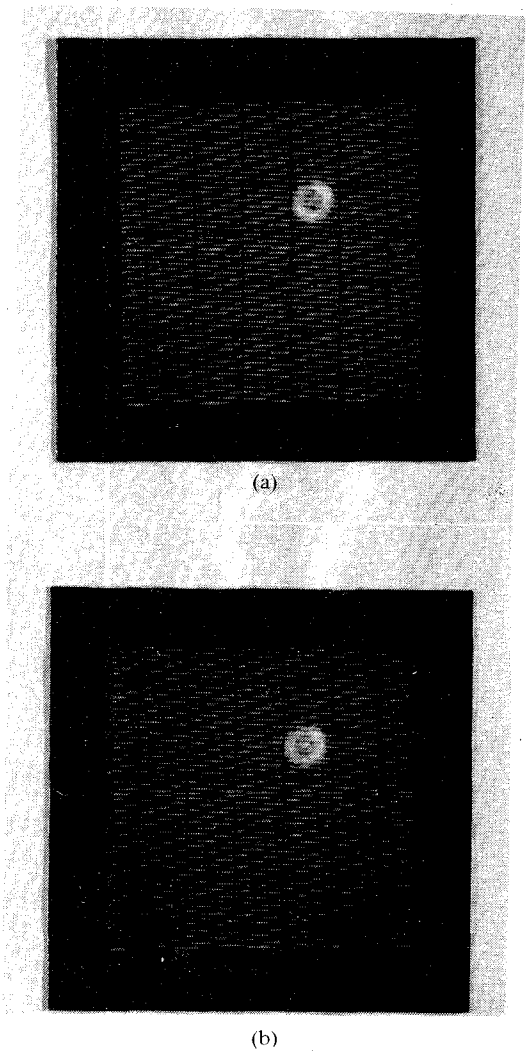

Fig. 4. The reconstructed microwave images from slices of (a) $\rho(\boldsymbol{p})/p$ and (b) $\Gamma(\boldsymbol{p})$ data measured in the frequency range 4–10 GHz.

position of the specular region when the T/R unit is at the other side. Therefore, the $\Gamma(\boldsymbol{p})$ data shown in Fig. 2(b) are symmetrical not only to $\theta = 45°$ but also to the center, whereas $\rho(\boldsymbol{p})/p$ data are symmetrical to $\theta = 45°$ only. However, they both yield images with the same feature showing the cylinder profile formed by specular regions as given in Fig. 4(a) and (b).

IV. Conclusions

In this paper, we have discussed the microwave images of a metallic convex object under physical optics approximations. It is shown that the image reconstructed from Bojarski's identity is the "edge-enhanced" version of the object characteristic function of the distribution of specular reflection regions. The same image can also be reconstructed from the range-normalized scattered far field using one-dimensional Fourier inversion and a back-projection algorithm.

References

[1] R. M. Lewis, "Physical optics inverse diffraction," *IEEE Trans. Antennas Propagat.*, vol. AP-24, pp. 308–314, May 1969.

[2] N. N. Bojarski, "A survey of physical optics inverse scattering identity," *IEEE Trans. Antennas Propagat.*, vol. AP-30, pp. 980–989, Sept. 1982.

[3] N. H. Farhat, C. L. Werner, and T. H. Chu, "Prospects for three-dimensional projective and tomographic imaging radar network," *Radio Sci.*, vol. 19, no. 5, pp. 1347–1355, Sept. 1984.

[4] W-M. Boerner, C. M. Ho, and B. Y. Foo, "Use of Radon's projection theory in electromagnetic inverse scattering," *IEEE Trans. Antennas Propagat.*, vol. AP-29, pp. 336–341, Mar. 1981.

[5] G. T. Ruck, D. E. Barrick, W. D. Stuart, and C. K. Krichbaum, *Radar Cross Section Handbook*. New York: Plenum, 1970.

[6] G. T. Herman, *Image Reconstruction from Projections — Implementation and Applications*. New York: Springer-Verlag, 1979.

[7] A. Papoulis, *Systems and Transforms with Applications in Optics*. New York: McGraw-Hill, 1968.

[8] D. C. Munson and J. L. C. Sanz, "Image reconstruction from frequency-offset Fourier data," *Proc. IEEE*, vol. 72, pp. 661–669, June 1984.

The Input Impedance of a Hollow-Probe-Fed, Semi-Infinite Rectangular Waveguide

JOHN M. ROLLINS AND JOHN M. JAREM, MEMBER, IEEE

Abstract **— Image theory is used to determine the input impedance of a coaxial feed in a short-circuited, semi-infinite rectangular waveguide. The analysis presented here is applicable to hollow antenna probes of variable height and lends itself well to accurate numerical evaluation. The numerical results are compared to results obtained from other methods and show the efficacy of using image theory to determine the waveguide input impedance.**

I. Introduction

A common problem in many microwave applications is the determination of the input impedance of a coaxially fed antenna probe in a rectangular waveguide. Several closed-form solutions [1], [2] of varying accuracy have been developed for the case where the waveguide is infinite in the forward and reverse directions of propagation. Considerable effort has also been expended in achieving input-impedance expressions for the case where one of the waveguide arms has been terminated with a short-circuiting plate, resulting in a semi-infinite waveguide geometry (Fig. 1).

In determining the input impedance of an infinite waveguide, one method, which has been pursued by Williamson [1], is the use of image theory to develop expressions for the electric and magnetic fields in the vicinity of the coaxial aperture. In his analysis, Williamson assumes perfect conductivity for the waveguide walls and shows that the system is equivalent to an infinite array of image sources which are treated as if they existed in free space and contributed to the fields affecting the primary waveguide feed (parent source). Each source, real or image, radiates fields which are due to a magnetic surface current in the annular region of its aperture and an electric surface current which flows on the surface of the probe. For the infinite waveguide shown in Fig. 1, Williamson obtains an expression for the admittance using a hollow probe of arbitrary height [1].

The introduction of a short circuit plate down the waveguide at a distance u from the center of the probe results in two arrays of probe and aperture images parallel to each other and separated by a distance $2u$. Each image is a source of radiating fields which are felt at the coaxial aperture and ultimately affect the input

Manuscript received October 30, 1987; revised June 28, 1988. This work was supported by Sandia National Laboratories, Albuquerque, NM 87185, under Contract 01-3817.

The authors are with the Department of Electrical Engineering, University of Texas at El Paso, El Paso, TX 79968.

IEEE Log Number 8927786.